An empirical potential-energy surface for the $He-I_2(B\,^3\Pi_u)$ van der Waals complex including three-body effects

A. García-Vela[a)]
Instituto de Matemáticas y Física Fundamental, Consejo Superior de Investigaciones Cientificas (CSIC), Serrano 123, 28006 Madrid, Spain

(Received 10 June 2005; accepted 1 August 2005; published online 28 September 2005)

An empirical intermolecular potential surface is proposed for the $He-I_2(B\,^3\Pi_u)$ complex, modeled as a sum of pairwise He–I Morse interactions plus a three-body interaction term. The potential reproduces with very good agreement the spectral blueshifts and vibrational predissociation lifetimes measured for $He-I_2(B,v')$ in the range $v'=10-67$ of I_2 vibrational excitations. In particular, the accuracy achieved in the description of the experimental data for high v' levels is attributed to the three-body interaction term included in the potential. The behavior of the potential surface with the I–I separation is analyzed and correlated with the experimental findings. © *2005 American Institute of Physics*. [DOI: 10.1063/1.2040367]

I. INTRODUCTION

The photodissociation dynamics of rare gas-halogen van der Waals (vdW) complexes has been an increasingly active subject of research over the last three decades. Even the simplest triatomic Rg-BC complexes (Rg=rare gas atom, BC =diatomic molecule) exhibit energy transfer processes and intramolecular vibrational redistribution (IVR) mechanisms which are fundamental in understanding the photophysics and photochemistry of molecules in solvated environments. Thus, the study of these simple clusters provides a detailed knowledge about the weak interactions which play a central role in the solvation effects present in larger, more complicated systems.

Potential-energy surfaces calculated by *ab initio* methods for the ground electronic state of several Rg-BC systems such as $He-Cl_2$,[1,2] $Ne-Br_2$,[3] $He-Br_2$,[4] and $He-I_2$ (Ref. 5) have been reported. The *ab initio* characterization of potential surfaces of excited electronic states is far more complicated for these systems, and fewer studies are available, among them those corresponding to $He-Cl_2$ (Ref. 6) and $He-Br_2$ (Ref. 7) for the B electronic state. More traditionally, the Rg-BC interaction in the B excited state has been described by empirical potential surfaces adjusted in order to reproduce the available spectroscopic and dynamical experimental data obtained from excitation and the subsequent vibrational predissociation (VP) process undergone by these complexes. In general, empirical intermolecular potentials consisting of a sum of two pairwise rare gas-halogen atom interactions (typically represented by Morse functions) have been able to reproduce successfully the available measurements.[8–12] However, the representation of the potential by pairwise interactions appears to be less satisfactory when the rare-gas atom weakly bound to the molecule is He. The $He-Cl_2(B)$ and $He-Br_2(B)$ complexes provide two examples.

Vibrational predissociation of $He-Cl_2(B,v')$ has been probed experimentally in the region of $v'=6-12$ initial vibrational states.[6,13–15] The empirical potentials proposed[14,15] reproduced well the observed spectral blueshifts and the vibrational and rotational Cl_2 product fragment distributions. The VP lifetime, however, was overestimated for the higher levels $v'=11,12$, and underestimated for the lower levels $v'<10$. In the case of $He-Br_2(B,v')$ a wider range of v' levels, $v'=8-48$, was investigated experimentally.[16–18] A $He-Br_2(B,v')$ empirical potential built up as an addition of pairwise interactions[19] reproduced successfully the measured spectral blueshifts and VP linewidths up to $v'\simeq 38$. The blueshift observed experimentally increases up to $v'\sim 35$, and then it decreases for higher v', suggesting that the vdW bond becomes stronger for high v' levels, which correspond to large Br–Br separations (>4.0 Å).[17] The decreasing behavior of the blueshift for high v' was not satisfactorily reproduced by the empirical pairwise potential proposed. In addition, the VP linewidths for $v'>38$ were also poorly described by the potential.

The above-mentioned results suggest that three-body effects may become important already for relatively low $v'=8-12$ levels in $He-Cl_2(B)$ and for high v' levels in $He-Br_2(B)$. The appearance of significant three-body effects would be related to the higher delocalization of the He atom in the complex (due to the quantum nature of He), as compared, for instance, to the cases of $Ne-Cl_2(B)$ and $Ne-Br_2(B)$. Because of this higher delocalization, the He atom would sample regions where the potential becomes more strongly dependent on the interhalogen separation.

In a recent work,[20] a $He-Cl_2(B)$ empirical potential was proposed which incorporated a three-body character by introducing an explicit dependence on the Cl–Cl separation in the potential parameters. Such a potential led to a substantial improvement in the description of the experimental VP lifetimes, as compared to previous empirical pairwise surfaces. The potential was also used in quantum-mechanical simulations of the $He_2-Cl_2(B)$ predissociation dynamics, providing

a)Electronic mail: garciavela@imaff.cfmac.csic.es

good agreement with the available measurements of linewidths and Cl_2 product rotational distributions[21(a)] and Cl_2 vibrational distributions.[21(b)] More recently, an empirical intermolecular potential for $He-Br_2(B)$ modeled as a sum of two pairwise He–Br interactions plus a three-body interaction term has been suggested.[22] Such a potential was able to reproduce the behavior of the blueshifts and linewidths observed experimentally for high v' states, in very good agreement with the measurements. The above two works show that including explicitly three-body effects in the potential surface is required in order to describe correctly the experimental data in this type of systems.

In light of the above results for $He-Cl_2(B)$ and $He-Br_2(B)$, it becomes very interesting to investigate the $He-I_2(B)$ complex. For this system, similarly as for $He-Br_2(B)$, there is an abundance of experimental data. Spectral blueshifts have been measured by Levy and coworkers up to $v'=29$ (Refs. 23 and 24) and by Sharfin *et al.*[25] in the range $v'=35-67$. Predissociation linewidths were also measured in the ranges $v'=12-26$ (Ref. 26) and $v'=35-66$ (Ref. 25) by means of frequency-resolved experiments. Time-resolved experiments were carried out by Gutmann *et al.*[27] and they obtained VP lifetimes in the region $v'=17-23$. These data cover most of the I_2 vibrational excitation spectrum in the B electronic state. Interestingly, the behavior of the spectral blueshift observed for $He-I_2(B)$ is similar to that found for $He-Br_2(B)$, namely, it increases up to $v'\sim 50$, and then a fast decrease occurs for higher v'.[25] Those results suggest a behavior of the $He-I_2(B)$ intermolecular potential qualitatively similar to the $He-Br_2(B)$ case, with a significant presence of three-body effects in the region of high v' levels.

An empirical potential surface was proposed for $He-I_2(B)$, represented as a sum of He–I Morse interactions.[28] The Morse parameters were fitted in order to reproduce the experimental linewidths available in the range $v'=12-23$.[26,27] The data of spectral blueshifts were not used in the fit. The aim of the present paper is to characterize a new empirical intermolecular potential for $He-I_2(B)$, which covers all the range of vibrational excitations, $v'=10-67$, probed experimentally. To this purpose, the potential surface is represented using the same model which worked successfully in the $He-Br_2(B)$ case[22] in order to take into account possible three-body effects. The corresponding potential parameters have been fitted using the available data for predissociation linewidths and spectral blueshifts in the above-mentioned range $v'=10-67$.

The organization of the paper is as follows. Section II describes the model used to represent the potential-energy surface and the calculations carried out to fit the potential parameters. In Sec. III the results are presented and the potential surface is discussed. Some conclusions are given in Sec. IV.

II. THE MODEL

A. Potential-energy surface

Jacobi coordinates (r,R,θ) are used to represent the $He-I_2$ system, where r is the I–I bond length, R is the distance between He and the I_2 center of mass, and θ is the angle between the vectors $\mathbf{r}$ and $\mathbf{R}$ associated with the two radial coordinates. As in the case of $He-Br_2(B)$,[22] the model used to represent the surface of $He-I_2(B)$ consists of a sum of three two-body interactions plus a three-body interaction term,

$$V(r,R,\theta)=V_{I_2}(r)+V_{\text{He-I}}(x_1)+V_{\text{He-I}}(x_2)+V_{3B}(r,x_1,x_2), \tag{1}$$

x_i being the He–I distances,

$$x_{1,2}=\left[\frac{r^2}{4}+R^2\pm rR\cos(\theta)\right]^{1/2}. \tag{2}$$

The analytical form reported in Ref. 29 has been used for the $V_{I_2}(r)$ interaction potential in the B electronic state.[30] The He–I interactions are represented by a Morse potential

$$V_{\text{He-I}}(x_i)=\epsilon_0\{\exp[-2\alpha_0(x_i-x_0)]-2\exp[-\alpha_0(x_i-x_0)]\}. \tag{3}$$

The three-body interaction term is modeled as a sum of two Morse functions of x_1 and x_2, respectively, where the Morse parameters are explicit functions of r,

$$\begin{aligned}V_{3B}(r,x_1,x_2)&=W(r,x_1)+W(r,x_2)\\&=\epsilon(r)\sum_{i=1}^{2}\{\exp[-2\alpha(r)(x_i-x_m(r))]\\&\quad-2\exp[-\alpha(r)(x_i-x_m(r))]\}.\end{aligned} \tag{4}$$

The above simple form of $V_{3B}(r,x_1,x_2)$ takes into account the symmetry of the interaction between the He atom and the two I atoms.

The decrease of the spectral blueshift found experimentally[25] for I_2 vibrational excitations higher than $v'\sim 50$, which corresponds with I–I bond lengths $r>5$ Å, suggests that three-body effects become important in this region of the potential. The decreasing shift indicates a strengthening of the vdW bond, and therefore suggests that the three-body interaction contributes to stabilize the potential with increasing r. Taking these features into account, the following functional forms have been used to model the three-body interaction term $V_{3B}(r,x_1,x_2)$,

$$\epsilon(r)=\epsilon_1\exp[-a_1(r-r_1)^2], \tag{5}$$

$$\alpha(r)=\alpha_0 \quad \text{if } r\leqslant r_2, \tag{6a}$$

$$\begin{aligned}\alpha(r)&=\alpha_0+\alpha_1\exp[-a_2(r-r_2)]\\&\quad\times\{\exp[-a_2(r-r_2)]-2\}+\alpha_1 \quad \text{if } r>r_2,\end{aligned} \tag{6b}$$

and

$$x_m(r)=x_0+x_3\exp[-a_3(r-r_3)^2]. \tag{7}$$

All the relevant parameters of the intermolecular potential are collected in Table I. The functions $\epsilon(r)$, $\alpha(r)$, and $x_m(r)$ are displayed in Fig. 1, along with the (squared) vibrational eigenfunctions of I_2 corresponding to $v'=10$ and $v'=67$, in order to show the range of I–I bond lengths probed by the experiment. It should be noted that the behavior of $\epsilon(r)$ en-

TABLE I. Potential parameters and atomic masses used in this work.

ϵ_0=14.94 cm^{-1}	a_2=0.983 $Å^{-1}$
α_0=1.293 $Å^{-1}$	a_3=0.354 $Å^{-2}$
x_0=4.05 Å	r_1=6.66 Å
ϵ_1=9.1 cm^{-1}	r_2=3.7 Å
α_1=0.37 $Å^{-1}$	r_3=6.85 Å
x_3=0.76 Å	m_{Br}=126.904 a.m.u.
a_1=0.857 $Å^{-2}$	m_{He}=4.003 a.m.u.

sures that the three-body term vanishes for very large I–I separations, causing the intermolecular potential to approach an isolated He–I interaction with increasing r, as expected.

B. Fit of the potential parameters

The parameters of the intermolecular potential of He–$I_2(B)$ were adjusted in order to reproduce the data available for spectral shifts and VP linewidths in the range v' = 10–67 of I_2 vibrational levels. All the spectroscopic and dynamical calculations carried out to fit the parameters assumed total angular momentum $J=0$ for the system.

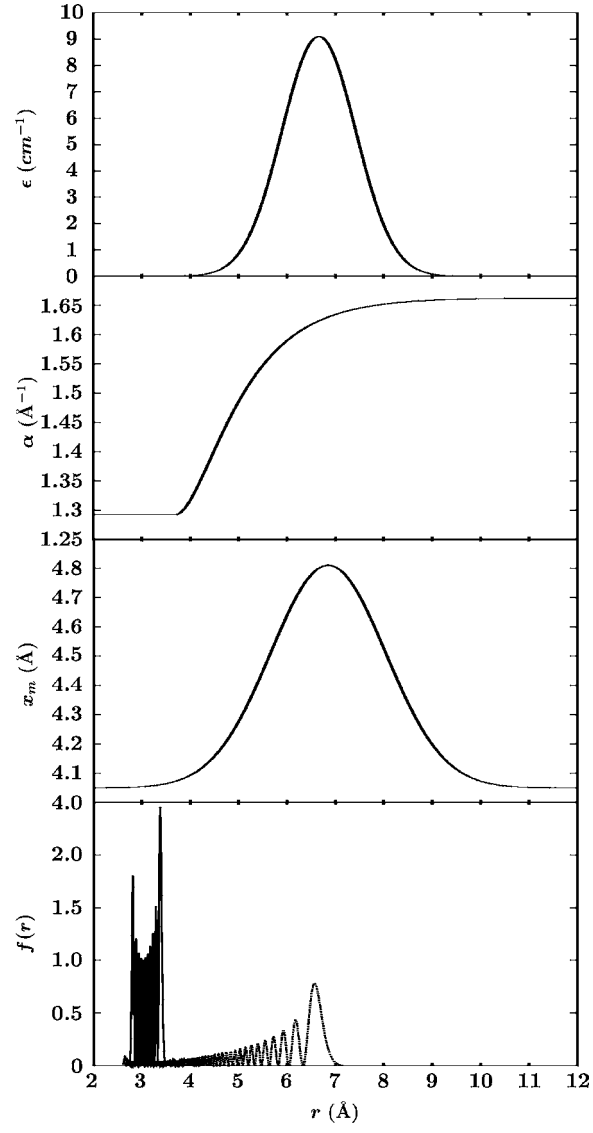

FIG. 1. Behavior of the ϵ, α, and x_m functions of Eqs. (5)–(7) vs the I–I distance r. The I_2 vibrational wave functions $|\chi_{v'}^{(j=0)}(r)|^2$ are also shown in the lower panel for $v'=10$ (solid line) and $v'=67$ (dashed line).

The blueshift of the He–$I_2(B,v') \leftarrow (X,v''=0)$ band origins can be obtained as the difference between the corresponding dissociation energies, $D_0(X,v''=0)-D_0(B,v')$. From the blueshift measurements for high v' levels,[25] the binding energy for the X state has been estimated as $D_0(X,v''=0)=17.6\pm1.0$ cm^{-1}.[17] Thus the value 17.6 cm^{-1} has been used here. The $D_0(B,v')$ dissociation energy corresponds to the energy of the ground resonance state of He–$I_2(B,v')$. The resonance wave function is expanded as

$$\Phi(r,R,\theta)=\sum_{n,j} c_{n,j}^{(v)}\psi_n^{(v)}(R)\chi_v^{(j)}(r)P_j(\theta), \tag{8}$$

where $\chi_v^{(j)}(r)$ are the rovibrational eigenstates of I_2, $P_j(\theta)$ are normalized Legendre polynomials, and $\psi_n^{(v)}(R)$ are radial basis functions. The $\psi_n^{(v)}(R)$ functions are obtained by calculating the eigenfunctions of the reduced Hamiltonian $\hat{H}_{vv}(R,\theta)=\langle\chi_v^{(j=0)}(r)|\hat{H}|\chi_v^{(j=0)}(r)\rangle$ [where $\hat{H}$ is the full Hamiltonian of He–$I_2(B)$] for several fixed angles θ, and then orthogonalizing these eigenfunctions through the Gram-Schmidt procedure. The resonance energy and wave function are obtained by representing the Hamiltonian $\hat{H}$ in the basis set of Eq. (8) and diagonalizing. Converged resonance energies were calculated by using a basis set of one vibrational state $v=v'$, $10\psi_n^{(v)}$ radial functions, and 15 Legendre polynomials (with even j).

The vibrational predissociation lifetimes are obtained from simulations of the decay dynamics of the complex ground resonance state, He–$I_2(B,v') \rightarrow$ He+$I_2(B,v<v')$. The simulations are carried out by solving the time-dependent Schrödinger equation for the wave packet $\Phi(r,R,\theta,t)$, which is expanded as

$$\Phi(r,R,\theta,t)=\sum_{v,j} C_{v,j}(R,t)\chi_v^{(j)}(r)P_j(\theta)e^{-iE_v^{(j)}t/\hbar}, \tag{9}$$

being $E_v^{(j)}$ the energies associated to the $\chi_v^{(j)}$ states. The coefficients $C_{v,j}(R,t)$ are propagated through a set of time-dependent coupled equations and they are represented on a uniform grid in the R coordinate consisting of 128 points with $R_0=3.5$ a.u. and $\Delta R=0.25$ a.u. The number of rotational states included in the expansion of Eq. (9) was 15 (with even j). In the vibrational basis, four vibrational states corresponding to $v=v'$, $v'-1$, $v'-2$, and $v'-3$ were included for the initial excitations $v'\leqslant 35$, while five vibrational states (adding $v=v'-4$ to the above states) were used for $v'=45$, six vibrational states (adding $v=v'-5$ to the above states) were used for $v'=51-61$, and seven vibrational states (adding $v=v'-6$ to the above states) were used for $v'\geqslant 65$. Absorption of the wave packet was carried out after each propagation time step by multiplying each $C_{v,j}(R,t)$ packet by the function $\exp[-A(R-R_{abs})^2]$, for $R>R_{abs}=28.0$ a.u., with $A=0.5$ $a.u.^{-2}$.

The $C_{v,j}(R,t)$ coefficients were propagated using the Chebychev polynomial-expansion method to express the evolution operator, with a propagation time step $\Delta t=0.04$ ps. Propagation was carried out until a different final

time t_f depending on the initial level v' being excited: $t_f = 80$ ps for $v'=12$, $t_f=70$ ps for $v'=13$, $t_f=60$ ps for $v'=14-45$, $t_f=52$ ps for $v'=51$, $t_f=30$ ps for $v'=54$ and 57, $t_f=24$ ps for $v'=61$, $t_f=20$ ps for $v'=65$, and $t_f=14$ ps for $v'=66$. The decay curve of the initial state population can be calculated as the square of the wave-packet autocorrelation function, $P(t)=|\langle\Phi(0)|\Phi(t)\rangle|^2$. By fitting $P(t)$ to an exponential function, $P(t)\simeq e^{-t/\tau}$, the predissociation lifetime τ of the $He-I_2(B,v')$ resonance state is obtained, which is related to the resonance linewidth Γ through $\Gamma=\hbar/\tau$. Vibrational and rotational state distributions of the I_2 fragment were calculated as previously described,[20,31] considering that the vdW bond is effectively broken for $R>R_c=16.6$ a.u.

As already mentioned, the present spectroscopic and dynamical calculations assume zero total angular momentum for the $He-I_2(B)$ complex. Although the measurements of the magnitudes used to fit the potential parameters are carried out at very low temperatures, transitions to $J>0$ states will have a weight. In addition, state mixing induced by Coriolis coupling terms present for $J>0$ might have some influence on the calculated predissociation lifetimes. Unfortunately, including such $J>0$ states in the fitting of the parameters would be extremely costly and would render the calculations impractical. However, it would be interesting to have an indication of how the $J=0$ assumption may affect the fit of the potential surface. This indication can be obtained from the related and extensively studied $He-Br_2(B)$ complex, for which different types of calculations have been carried out. Spectral shifts were calculated for $He-Br_2(B,v')$ in the $v'=8-20$ range, both assuming $J=0$ (Ref. 19) and including states up to $J\leqslant 6$.[18] The two types of calculations gave blueshifts with differences between them and with the experimental ones typically smaller than 1%. Regarding dynamical quantities, rotational distributions of the Br_2 product fragment were computed by means of line-shape calculations including transitions to $J\leqslant 5$ states of $He-Br_2(B)$ (Ref. 32) using a B state potential surface previously fitted through line-shape calculations assuming $J=0$.[19] Good agreement was found between the calculated and measured Br_2 rotational distributions.[32] The above results seem to indicate that fitting the potential parameters under the assumption of $J=0$ is a reasonably good approximation.

III. RESULTS AND DISCUSSION

A. Spectral shifts and predissociation lifetimes

Analysis of the calculated ground resonance wave functions shows that they are localized around $\theta=90°$, in the perpedicular configuration of the complex, for the whole range $v'=10-67$. The corresponding ground resonance energies of $He-I_2(B,v')$, $E_{\rm res}^{\rm calc}$, are listed in the third column of Table II. Spectral shifts obtained from these energies are collected in the fourth column of the table. The experimental blueshifts are given in the last two columns with the reported errors.[23–25] In Fig. 2 the calculated and experimental blueshifts are plotted vs v'.

The blueshifts calculated with the present empirical potential display an excellent, quantitative agreement with the experimental ones, in the whole range of v' levels studied. The computed blueshifts are within the experimental error bars or very close to their limits. In this sense, it is noted that the maximum experimental error reported is about ±1.5%, being typically smaller for most of the v' levels measured.

Dynamical quantities such as the predissociation lifetimes are sensitive to more extensive regions of the potential than the spectral shifts. The reason is that during the dynamics the system decays to lower vibrational manifolds $v<v'$ ($v=v'-1$, $v'-2$, $v'-3$, etc.), and the short- and long-range regions of the potential in those vibrational states are sampled. Thus, a good description of the dynamical magnitudes measured is indicative of the quality of the potential surface. The calculated lifetimes are collected in Table III, along with the experimental ones with the reported errors. Both the calculated and experimental lifetimes are also plotted in Fig. 3.

As mentioned in Sec. II B, in order to extract the VP lifetime the decay curve $P(t)$ is fitted to an exponential function $e^{-t/\tau}$. The underlying assumption in a single exponential fit of $P(t)$ is that the resonance state initially prepared is isolated. In the case of $He-I_2(B,v')$ such a regime is found for $v'\leqslant 45$. For $v'\geqslant 51$ the $He-I_2(B,v')$ resonance initially excited appears to interact with other metastable states close in energy, belonging to vibrational manifolds $v<v'$. This interaction between resonances of different vibrational manifolds manifests itself in the $P(t)$ curve which, after an initial decay, shows one or more recurrences. In this multiexponential dynamics regime the decay curve $P(t)$ can no longer be fitted to a single exponential function. Actually, the same behavior was found in the case of $He-Br_2(B,v')$ for high v',[19,22] and it was attributed to possible intramolecular vibrational relaxation mechanisms.[19] With increasing v' the width of the initial resonance state increases as well, and thus the probability of overlapping and interaction between this resonance and other $v<v'$ resonances energetically close is expected to increase.

In order to obtain the lifetime of the $He-I_2(B,v')$ resonance of interest for $v'\geqslant 51$, the same procedure applied previously[22] in the case of $He-Br_2(B,v')$ was used here. It consisted of neglecting the recurrences and fitting only the initial decay of $P(t)$ to a single exponential, in the assumption that in the absence of interaction between resonances the recurrences would not appear. In Fig. 4 two typical decay curves corresponding to the multiexponential regime are shown for the $v'=54$ and 61 I_2 excitations, along with their exponential fits. As seen from the figure, the intensity of the recurrences is rather low and they appear after the population curve has decayed almost completely. Thus, the time scale of decay of the curve (within the first 8 ps), associated with the decay of the resonance initially excited, is well separated from the time scale of appearance of the recurrences. This allows one to extract a sufficiently accurate lifetime for the resonance of interest by fitting the initial decay of the population to a single exponential function.

In general, the vibrational dependence of the lifetimes found experimentally is very well reproduced by the calculated lifetimes in the whole v' range probed. For the levels $v'=17-23$ there are some discrepancy between the lifetimes measured in the frequency-resolved[26] and in the

TABLE II. Experimental and calculated spectral blueshifts of He–$I_2(B,v')$. The calculated He–$I_2(B,v')$ ground resonance energies (relative to the initial I_2 vibrational energy level $E_{v'}^{j=0}$) are listed in the third column. $E_{v'}^{j=0}=0$ corresponds to separated I atoms.

			Blueshift (cm^{-1})		
v'	$E_{v'}^{j=0}$ (cm^{-1})	E_{res}^{calc} (cm^{-1})	This work	Expt.[a]	Expt.[b]
10	−3145.87	−13.976	3.62	3.58	
12	−2931.80	−13.954	3.65		
13	−2827.47	−13.942	3.66	3.60±0.04	
14	−2724.97	−13.930	3.67	3.68±0.02	
15	−2624.32	−13.917	3.68	3.66±0.02	
16	−2525.53	−13.905	3.70	3.70±0.04	
17	−2428.63	−13.891	3.71	3.73±0.02	
18	−2333.64	−13.878	3.72	3.73±0.05	
19	−2240.56	−13.864	3.74	3.75±0.02	
20	−2149.41	−13.849	3.75	3.76±0.04	
21	−2060.22	−13.834	3.77	3.80±0.02	3.79±0.05
22	−1972.99	−13.818	3.78	3.81±0.02	
23	−1887.73	−13.802	3.80	3.86±0.03	
24	−1804.46	−13.786	3.81	3.87±0.04	
25	−1723.19	−13.769	3.83	3.90±0.02	
26	−1643.94	−13.751	3.85	3.91±0.04	
29	−1418.31	−13.695	3.91	3.97	
35	−1022.14	−13.563	4.04		4.06±0.05
45	−523.92	−13.297	4.30		
47	−447.75	−13.246	4.35		4.37±0.05
51	−317.44	−13.186	4.41		
54	−237.94	−13.222	4.38		
57	−172.87	−13.385	4.21		4.25±0.05
61	−106.38	−13.833	3.77		3.77±0.05
65	−59.95	−14.529	3.07		
66	−51.05	−14.698	2.90		2.88±0.05
67	−43.12	−14.768	2.83		2.8

[a]References 23 and 24.
[b]Reference 25.

time-resolved[27] experiments. In this region the calculated lifetimes are typically between the data of the two experiments. Good agreement is also found for $v' \geq 35$, except for the last two vibrational levels, $v'=65$ and 66, where the deviation is larger. The experiment finds a gradual increase of the lifetime between $v'=57$ and $v'=66$,[25] and this behavior is not well reproduced by the theoretical lifetimes. The present potential surface appears to overestimate to some extent the coupling between the I_2 vibration and the vdW modes for $v'>61$, leading to a faster predissociation dynamics.

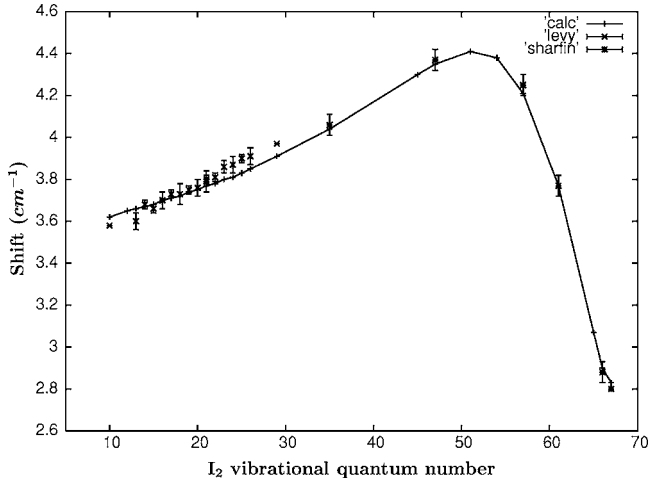

FIG. 2. Experimental and calculated spectral blueshifts of He–$I_2(B,v')$ vs the I_2 vibrational excitation v'. (+) This work; (×) data of Levy and coworkers (Refs. 23 and 24); (*) data of Sharfin *et al.* (Ref. 25). See the text for details.

It should be noted that the three-body interaction term becomes effective for $r>4$ Å (see the top panel of Fig. 1). Thus, for smaller I–I bond lengths (corresponding to vibrational excitations lower than $v' \sim 45$), the potential surface of Eq. (1) consists essentially of a sum of atom-atom interactions. The good level of description achieved for the spectral shifts and predissociation lifetimes for $v'<45$ indicates that a representation of the potential based on pairwise interactions is good enough in this region of v' excitations.

B. Vibrational and rotational state distributions

The calculated vibrational distributions of the $I_2(B,v<v')$ product fragment show that the $\Delta v'=-1$ dissociation channel is dominant for vibrational excitations $v' \leq 57$ (with a population >90% for $v' \leq 26$). For $v' \geq 61$ the $\Delta v'=-2$ channel becomes dominant, and the $\Delta v'=-1$ vibrational

TABLE III. Experimental and calculated vibrational predissociation lifetimes of $He-I_2(B,v')$.

	Lifetime (ps)			
v'	This work	Expt.[a]	Expt.[b]	Expt.[c]
12	223.0	221±20		
13	209.0	171±3		
14	185.3	153±9		
15	151.0	153±9		
16	123.0	121±4		
17	110.0	104±2	128±2	
18	109.0	94±1	115±9	
19	102.0	85±3	101±4	
20	83.4	76±2	94±4	
21	66.3	69±1	82±4	
22	61.1	60±2	75±6	
23	63.5	51.9±0.7	65±5	
24	58.5	47.7±0.9		
25	44.7	42.7±0.5		
26	36.7	37.9±1.3		
35	17.5			17.8
45	6.7			8.6
51	3.9			4.8
54	3.1			3.6
57	2.5			2.4
61	2.5			3.2
65	1.7			3.8
66	1.4			4.1

[a]Reference 26.
[b]Reference 27.
[c]Reference 25.

channel is energetically closed for $v' \geq 62$. For $v' \geq 61$ the dissociation channels $\Delta v' = -4$, -5, and -6 reach significant populations.

Rotational state distributions of the $I_2(B, v < v', j)$ fragment were calculated (for even j). In Fig. 5 the rotational distributions corresponding to the $\Delta v' = -1$ and -2 channels are shown for several v' excitations along the range studied

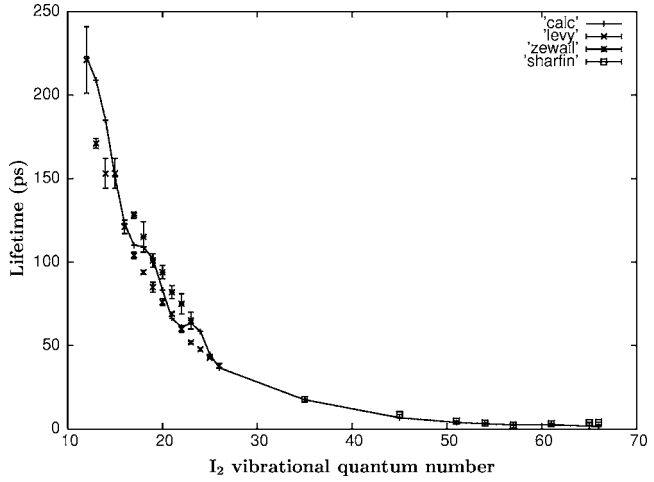

FIG. 3. Experimental and calculated predissociation lifetimes of $He-I_2(B,v')$ vs the I_2 vibrational excitation v'. (+) This work; (×) data of Johnson *et al.* (Ref. 26); (∗) data of Gutmann *et al.* (Ref. 27); (□) data of Sharfin *et al.* (Ref. 25).

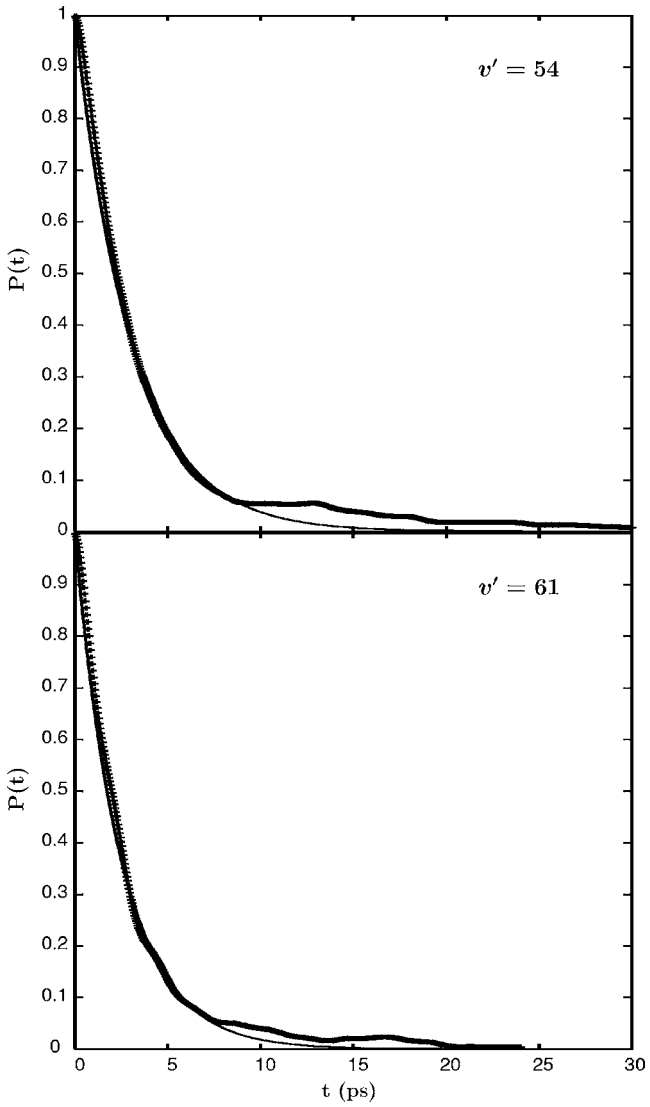

FIG. 4. Calculated decay curves of the $He-I_2(B,v')$ ground resonance state (+) and the corresponding exponential fits (solid lines) vs time for $v'=54$ and $v'=61$.

(in the case of $v'=65$ the $\Delta v'=-1$ channel is closed, and the distributions correspond to the $\Delta v'=-2$ and -3 channels). In general, for $v' \leq 45$ the $\Delta v'=-1$ and -2 distributions are rather similar, the $\Delta v'=-2$ rotational distributions being somewhat hotter. The rotational distributions for $v' \leq 45$ typically consist of a main peak at $j=2$ and one or two secondary peaks. These distributions are qualitatively similar to the $\Delta v'=-1$ and -2 rotational distributions found for the $Cl_2(B, v < v')$ fragment after $He-Cl_2(B)$ predissociation.[20]

For $v' > 51$ the $\Delta v'=-2$ rotational distribution (and also the $\Delta v'=-3$ distribution) of I_2 develops a pronounced structure of peaks. The $\Delta v'=-2$ distributions for $v' > 51$ also exhibit a higher rotational excitation as compared to the $\Delta v'=-2$ distributions corresponding to $v' < 51$, despite the smaller amount of energy available as v' increases. The structure and the higher excitation might be related to the interaction between the resonance initially prepared and other resonances belonging to lower $v < v'$ vibrational manifolds.

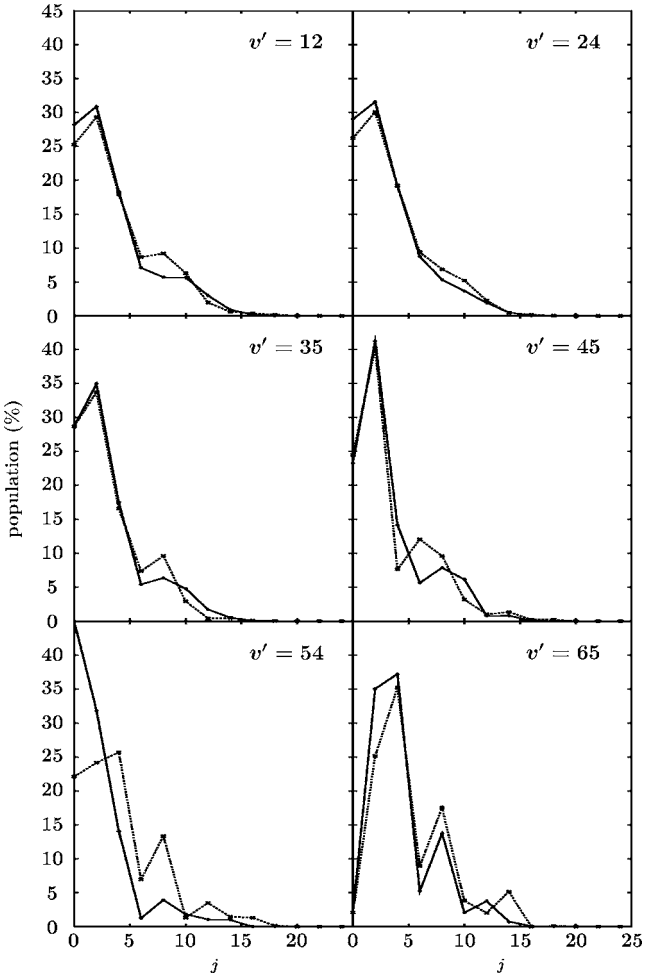

FIG. 5. Calculated $I_2(B,v,j)$ fragment rotational distributions after vibrational predissociation of He–$I_2(B,v')$ through the $v=v'-1$ (solid line) and $v=v'-2$ (dashed line) channels. In the case of $v'=65$ the distributions correspond to the $v=v'-2$ (solid line) and $v=v'-3$ (dashed line) dissociation channels.

C. Analysis of the potential surface

The agreement found between the calculated and the experimental spectral shifts and predissociation lifetimes indicates that the He–$I_2(B)$ interaction is well described by the present potential surface, at least in the range of I–I separations explored by the experiment (3 Å $< r <$ 7 Å). In the following, the details of the potential and its dependence on the internuclear I–I separation will be analyzed. Table IV presents the energy and position of the potential minima in the linear ($\theta=0°$) and perpendicular ($\theta=90°$) configurations of the complex for several I–I bond lengths.

Between $r=3.1$ and $r=4.0$ Å, the minimum energy decreases slightly in the linear configuration, while in the perpendicular configuration it remains rather constant around -29.9 cm^{-1}. For $r>4.0$ Å the attractive three-body interaction is already effective and the energy minimum becomes gradually deeper in both the linear and the perpendicular configurations, the well depth reaching a maximum around $r=6.5$ Å. For larger I–I separations the well depth decreases in the two configurations, approaching the value corresponding to the He–I pairwise interaction.

The position of the potential minimum in the linear configuration, $R^{\min}(\theta=0°)$, increases monotonically with r in the whole range of I–I bond distances. On the contrary, in the perpendicular configuration $R^{\min}(\theta=90°)$ decreases with increasing r up to about $r=6.5$ Å, where a slight increase takes place, and then it turns to decrease again for larger r, reaching the value $R^{\min}(\theta=90°)=0$ Å for distances $r \geqslant 8.5$ Å. This behavior indicates that in the T-shaped configuration, as the I–I bond elongates, the He atom gradually approaches the middle position between the two I atoms. The same result was found in the case of the He–$Br_2(B)$ complex.[22]

Another similarity with He–$Br_2(B)$ is that for $r \geqslant 9.5$ Å the absolute minimum of the potential lies no longer in the T-shaped configuration, but rather in the linear geometry at short $R^{\min}(\theta=0°)$ distance. Table IV shows that for $r=10.0$ Å the absolute minimum $V^{\min}(\theta=0°)=-17.50$ cm^{-1} occurs at $R^{\min}(\theta=0°)=0.87$ Å. For such a large I–I bond length, an optimal interaction of He and the I atoms is achieved when He is between the two I atoms, but somewhat closer to one of them. The same behavior was exhibited by the He–$Br_2(B)$ interaction potential[22] for Br–Br separations $r \geqslant 9.0$ Å. It should be noted from Table IV that, in the linear configuration, the absolute minimum of energy is deeper at a large distance such as $r=10.0$ Å than at $r=3.1$ Å.

Contour plots of the He–$I_2(B)$ interaction potential are shown in Figs. 6 and 7 for several I–I bond distances. The contour shows the gradual deepening of the potential well with increasing I–I bond length and how He approaches a position between the two I atoms. This behavior is qualitatively the same as that presented by the He–$Br_2(B)$ intermolecular potential, with the difference that in the He–$Br_2(B)$ case He approaches more rapidly a position between the Br atoms as the interhalogen separation increases.[22] The deepening of the He–$I_2(B)$ potential well with increasing r is consistent with a strengthening of the vdW bond and with the decrease of the spectral blueshift found experimentally[25] for high v' levels.

TABLE IV. Energies and positions of the potential minima in the linear ($\theta=0°$) and perpendicular ($\theta=90°$) configurations of He–$I_2(B)$ for several I–I separations. The numbers in parentheses for $r=10.0$ Å correspond to the absolute potential minimum in the linear configuration. See the text for details.

r (Å)	3.1	3.5	4.0	5.0	6.5	7.5	10.0
$V^{\min}(\theta=0°)$(cm^{-1})	−15.48	−15.27	−15.13	−15.72	−19.04	−16.21	−14.94(−17.50)
$V^{\min}(\theta=90°)$(cm^{-1})	−29.88	−29.88	−29.92	−31.36	−38.07	−32.42	−14.94
$R^{\min}(\theta=0°)$(Å)	5.59	5.79	6.04	6.57	7.88	8.25	9.05(0.87)
$R^{\min}(\theta=90°)$(Å)	3.74	3.65	3.52	3.22	3.30	2.48	0.0

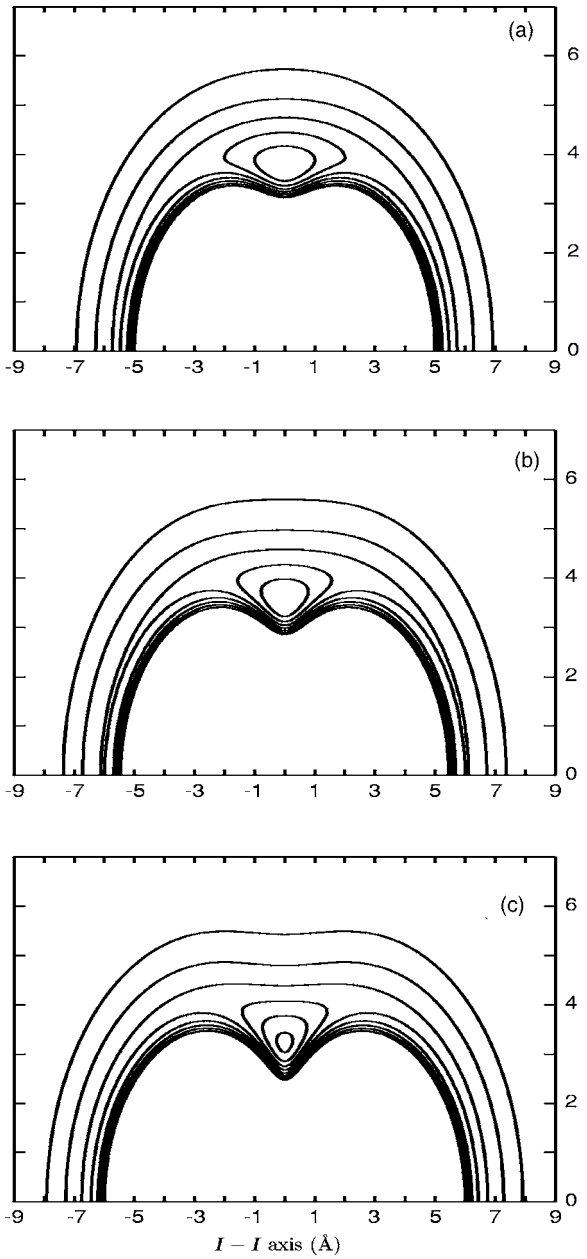

FIG. 6. Contour plots of the $He-I_2(B,v')$ empirical potential surface for three I–I separations, $r=3.1$ Å (a), $r=4.0$ Å (b), and $r=5.0$ Å (c). The spacing between the contours is 5 cm^{-1} starting from the outermost contour at -5 cm^{-1}, and the units are Å on both axis of the plot. For $r=3.1$, 4.0, and 5.0 Å, the I atoms are located at ±1.55, ±2.0, and ±2.5 Å, respectively, on the horizontal axis of the plot.

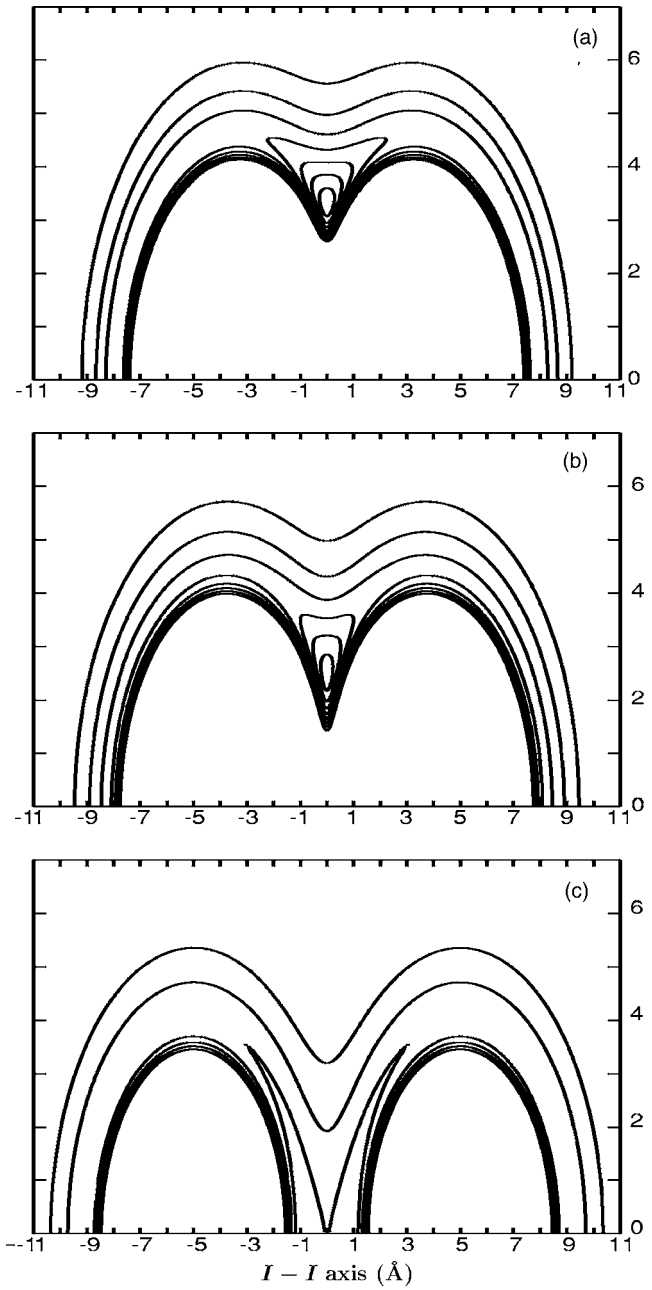

FIG. 7. Same as Fig. 6 but for the I–I separations $r=6.5$ Å (a), $r=7.5$ Å (b), and $r=10.0$ Å (c), for which the I atoms are located at ±3.25, ±3.75, and ±5.0 Å, respectively, on the horizontal axis of the plot.

Figures 6 and 7 also show that the intermolecular potential exhibits a stronger dependence on the I–I separation in the range $5.0\ \text{Å} < r < 7.5\ \text{Å}$ (i.e., for $v' > 50$) than in the $3.1\ \text{Å} < r < 5.0\ \text{Å}$ range. This result is related with the appearance of increasingly important three-body effects as r increases, and it is consistent with the behavior observed experimentally for the blueshift, which increases up to $v' \sim 50$, and then it reverses the trend, decreasing for higher v'.

IV. CONCLUSIONS

An empirical intermolecular potential surface for the $He-I_2(B)$ complex is proposed, which is represented by a sum of atom-atom Morse He–I interactions plus a three-body interaction term. The potential reproduces with very good agreement the spectral shifts and predissociation lifetimes measured in a wide range of I_2 vibrational excitations, $v' = 10-67$. This is the first $He-I_2(B)$ potential surface which covers such a large range of v' excitations. In particular, the behavior of the spectral blueshift observed experimentally, consisting of an increase of up to $v' \sim 50$, and then a sharp decrease for higher v' levels, is accurately described by the potential surface. The accuracy achieved in the description of the experimental data for high v' is attributed to the attractive three-body interaction term included in the potential surface.

The present interaction potential predicts the T-shaped

configuration of He–$I_2(B)$ to be the equilibrium one in most of the range of I–I separations. As the interhalogen separation increases, the He atom approaches a middle position between the two I atoms, causing a strengthening of the vdW bond consistent with the experimental findings. For large I–I separations ($\geqslant$8.5 Å) the complex is predicted to become linear, with He just in the middle of the I–I bond axis or somewhat closer to one of the I atoms. The behavior of the He–$I_2(B)$ interaction potential with the interhalogen separation is qualitatively similar to that exhibited by the He–$Br_2(B)$ intermolecular potential. This is in agreement with the qualitatively similar vibrational dependence of the spectral blueshifts and predissociation lifetimes observed experimentally for the two complexes. Finally, the present model used to represent the interaction potential has proven to be successful in describing the spectroscopy and dynamics of this type of systems in the region of large interhalogen separations where three-body effects become important.

ACKNOWLEDGMENTS

This work was supported by C.I.C.Y.T. (Ministerio de Educación y Ciencia), Spain, Grant No. FIS-2004-02461. The Centro de Supercomputación de Galicia (CESGA) and the Grupo de SuperComputación del CIEMAT (GSC) are acknowledged for allocation of computer time.

[1] G. Chalasiński, M. Gutowski, M. M. Szczęśniak, J. Sadlej, and S. Scheiner, J. Chem. Phys. **101**, 6800 (1994).
[2] S. M. Cybulski and J. S. Holt, J. Chem. Phys. **110**, 7745 (1999).
[3] R. Prosmiti, C. Cunha, P. Villarreal, and G. Delgado-Barrio, J. Chem. Phys. **116**, 9249 (2002).
[4] A. Valdés, R. Prosmiti, P. Villarreal, and G. Delgado-Barrio, Mol. Phys. **102**, 2277 (2004).
[5] R. Prosmiti, A. Valdés, P. Villarreal, and G. Delgado-Barrio, J. Phys. Chem. A **108**, 6065 (2004).
[6] J. Williams, A. Rohrbacher, J. Seong *et al.*, J. Chem. Phys. **111**, 997 (1999).
[7] M. P. de Lara Castells, A. A. Buchachenko, G. Delgado-Barrio, and P. Villarreal, J. Chem. Phys. **120**, 2182 (2004).
[8] N. Halberstadt, J. A. Beswick, and K. C. Janda, J. Chem. Phys. **87**, 3966 (1987).
[9] S. K. Gray and C. E. Wozny, J. Chem. Phys. **91**, 7671 (1989); **94**, 2817 (1991).
[10] T. A. Stephenson and N. Halberstadt, J. Chem. Phys. **112**, 2265 (2000).
[11] A. García-Vela, J. Phys. Chem. A **106**, 6857 (2002).
[12] S.-S. Cho and H. Sun, Chem. Phys. Lett. **377**, 406 (2003).
[13] J. I. Cline, D. D. Evard, F. Thommen, and K. C. Janda, J. Chem. Phys. **84**, 1165 (1986).
[14] J. I. Cline, B. P. Reid, D. D. Evard, N. Sivakumar, N. Halberstadt, and K. C. Janda, J. Chem. Phys. **89**, 3535 (1988).
[15] L. Beneventi, P. Casavecchia, G. G. Volpi, C. R. Bieler, and K. C. Janda, J. Chem. Phys. **98**, 178 (1993).
[16] L. J. van de Burgt, J.-P. Nicolai, and M. C. Heaven, J. Chem. Phys. **81**, 5514 (1984).
[17] D. G. Jahn, S. G. Clement, and K. C. Janda, J. Chem. Phys. **101**, 283 (1994).
[18] D. G. Jahn, W. S. Barney, J. Cabalo *et al.*, J. Chem. Phys. **104**, 3501 (1996).
[19] T. González-Lezana, M. I. Hernández, G. Delgado-Barrio, A. A. Buchachenko, and P. Villarreal, J. Chem. Phys. **105**, 7454 (1996).
[20] A. García-Vela, J. Chem. Phys. **119**, 5583 (2003).
[21] (a) A. García-Vela, J. Chem. Phys. **122**, 14312 (2005); (b) **122**, 216101 (2005).
[22] A. García-Vela, J. Phys. Chem. A **109**, 5545 (2005).
[23] J. E. Kenny, K. E. Johnson, W. Sharfin, and D. H. Levy, J. Chem. Phys. **72**, 1109 (1980).
[24] J. A. Blazy, B. M. Dekoven, T. D. Russell, and D. H. Levy, J. Chem. Phys. **72**, 2439 (1980).
[25] W. Sharfin, P. Kroger, and S. C. Wallace, Chem. Phys. Lett. **85**, 81 (1982).
[26] K. E. Johnson, L. Wharton, and D. H. Levy, J. Chem. Phys. **69**, 2719 (1978).
[27] M. Gutmann, D. M. Willberg, and A. H. Zewail, J. Chem. Phys. **97**, 8037 (1992).
[28] S. K. Gray, Faraday Discuss. **97**, 143 (1994).
[29] M. Gruebele and A. H. Zewail, J. Chem. Phys. **98**, 883 (1993).
[30] Note that there is a typesetting error in Eq. (17) of Ref. 29. In that paper the expression of q_1 reads $q_1=2.9343\times10^{-3}(D/Z)^2p_0$ and should instead read $q_1=2.9343\times10^{-3}(D/Z^2)^{1/2}p_0$ [A. H. Zewail (private communication)].
[31] M. Ceotto and A. García-Vela, J. Chem. Phys. **115**, 2146 (2001).
[32] A. Rohrbacher, T. Ruchti, K. C. Janda, A. A. Buchachenko, M. I. Hernández, T. González-Lezana, P. Villarreal, and G. Delgado-Barrio, J. Chem. Phys. **110**, 256 (1999).